

RESEARCH ARTICLE

10.1002/2014JC009951

Key Points:

- A new ecosystem model with nitrogen and phosphorus limitation was developed
- The effect of phosphorus limitation on a plume ecosystem was investigated
- The N:P ratio and the effect of phosphorus limitation vary along the plume

Correspondence to:

J. Gan,
magan@ust.hk

Citation:

Gan, J., Z. Lu, A. Cheung, M. Dai, L. Liang, P. J. Harrison, and X. Zhao (2014), Assessing ecosystem response to phosphorus and nitrogen limitation in the Pearl River plume using the Regional Ocean Modeling System (ROMS), *J. Geophys. Res. Oceans*, 119, doi:10.1002/2014JC009951.

Received 7 MAR 2014

Accepted 25 NOV 2014

Accepted article online 28 NOV 2014

Assessing ecosystem response to phosphorus and nitrogen limitation in the Pearl River plume using the Regional Ocean Modeling System (ROMS)

Jianping Gan¹, Zhongming Lu¹, Anson Cheung¹, Minhan Dai², Linlin Liang¹, Paul J. Harrison³, and Xiaozheng Zhao¹

¹Department of Mathematics and Division of Environment, Hong Kong University of Science and Technology, Kowloon, Hong Kong, ²State Key Laboratory of Marine Environmental Science, Xiamen University, Xiamen, China, ³Department of Earth and Ocean Sciences, University of British Columbia, Vancouver, British Columbia, Canada

Abstract The effect of phosphorus limitation on the Pearl River plume ecosystem, where large gradients in both nitrogen (N) and phosphorus (P) concentrations exist, is investigated in this process-oriented study by coupling the Regional Ocean Modeling System (ROMS) model with a new nitrogen, phosphorus, phytoplankton, zooplankton, and detritus (NPPZD) ecosystem model. The results of the N-based only model of Gan et al. (2010) were compared with those of the new NP-based model for the plume. The inclusion of P-limitation noticeably reduces the total phytoplankton production in the plume in the P-limited near and midfield regions of the plume. However, the nitrate in the plume extends farther downstream and forms a broad area of phytoplankton bloom in the N-limited far field. Moreover, it changes the photosynthetically active radiation and strengthens the subsurface chlorophyll maximum in the near and midfields, but weakens it in the far field. A high N:P ratio of ~ 120 in the near field decreases quickly to a low N:P ratio of < 13.3 in the far field due to a higher N:P consumption ratio and mixing with ambient waters with a lower N:P ratio. Mortality and coagulation acts as major sinks for phytoplankton production in the near and midfield during the developmental stage of the bloom, but grazing gradually becomes the most important sink for phytoplankton production in the entire plume during the mature stage. It was shown that the magnitudes of the difference between the NP-based and N-based cases decrease sequentially for nutrients, phytoplankton, and zooplankton.

1. Introduction

Nutrient limitation in the aquatic ecosystem is generally defined as the limitation of the potential rate of net primary production, or when the net primary production will increase if the limiting nutrient is added. The molar ratio of dissolved inorganic nitrogen (DIN) and dissolved inorganic phosphate (DIP) concentrations (N:P ratio) has often been used as an indicator of nutrient limitation. A N:P ratio $< 16:1$ indicates N limitation, while a N:P ratio $> 16:1$ reveals P limitation [Redfield, 1958]. The absolute concentration of each nutrient is also very important to indicate which nutrient is limiting. If the concentration of DIN and DIP are both very low, the ecosystem could be co-limited; on the contrary, if both DIN and DIP are very high (i.e., $\text{DIN} > 2 \text{ mmol m}^{-3}$ and $\text{DIP} > 0.2 \text{ mmol m}^{-3}$), there will be no nutrient limitation even if the N:P ratio deviates from the Redfield ratio. In general, nitrogen is thought to be limiting in most marine systems [Howarth, 1988]. However, in the land-sea transitional zone such as the river plume, previous studies [e.g., Harrison et al., 1990; Fong et al., 1993; Guillard et al., 2000] have revealed that for rivers with a high N load, there is a shift to P limitation in the near field (near the entrance of the estuary) and N limitation in the far field (downstream of the plume).

The Pearl River plume is formed by the Pearl River discharge into coastal waters. In summer, a high discharge rate of $\sim 16,000 \text{ m}^3 \text{ s}^{-1}$ [Cai et al., 2004; Lu and Gan, 2014] and concurrent coastal upwelling circulation [Gan et al., 2009a] spread the plume over the broad continental shelf in the northeastern South China Sea (NSCS, Figure 1). The terrestrial freshwater input provides a rich nutrient source for phytoplankton blooms in the plume [Gan et al., 2010; Lu et al., 2010], despite the fact that the oligotrophic South China Sea (SCS) has extremely low nutrient concentrations in the surface water [Wu et al., 2003]. The ecosystem in this plume-affected region is potentially P-limited [Chen et al., 2002; Xue and Chai, 2001; Xu et al., 2008]. In the NSCS, the surface water N:P ratio in the outer shelf is < 10 , but > 100 in the Pearl River Estuary (PRE) and in

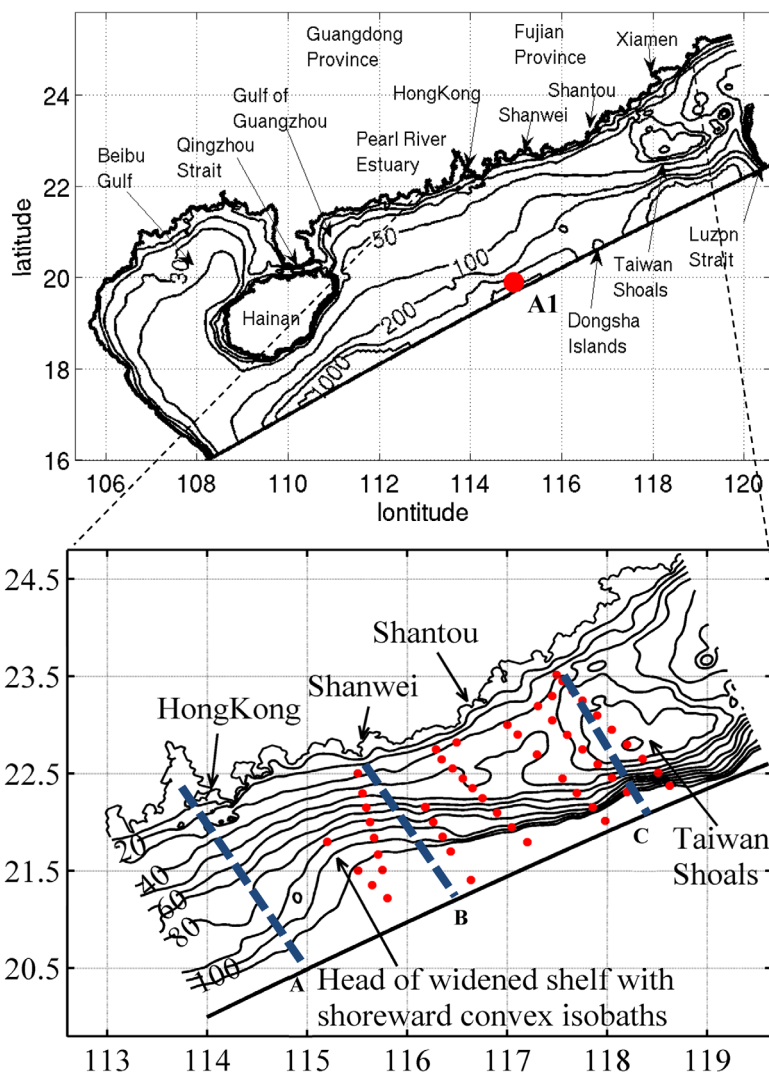


Figure 1. The bathymetry (in meter) of the northwestern South China Sea and the zoomed area is the region between Guangdong and Xiamen. The selected cross-shelf transects (blue dashed lines) are denoted as A, B, and C. The survey stations are indicated by solid red circles.

the plume over the adjacent shelf [Cai *et al.*, 2004; Harrison *et al.*, 2008; Ning *et al.*, 2004; Yin, 2002; Zhang, 2000]. Thus, there is a shift from N deficit in the outer shelf to P deficit in the plume near shore. However, most of these previous studies, like many in the other parts of the world's ocean, are largely constrained by spatiotemporally limited field measurements and a comprehensive analysis of the P-limited effects on the ecosystem over the entire plume-affected region in the NSCS has not been conducted.

In an earlier study by Gan *et al.* [2010], a nitrogen-based (N-based) biological model was used to simulate the ecosystem responses to the wind-driven summer upwelling and the Pearl River plume in the NSCS. The model simulations were based only on N, and overestimated the pelagic biomass and primary production in this region. However, in this paper, we developed a new nitrogen, phosphorus, phytoplankton, zooplankton, and detritus (NPPZD) ecosystem model and coupled it with a three-dimensional circulation model to study both N-limited and P-limited ecosystems in the Pearl River plume and beyond. No other numerical modeling study has investigated the effect of P limitation in the river plume on the pelagic ecosystem in the NSCS.

There are mainly two types of approaches in biological models that address the multiple nutrient limitations in an aquatic ecosystem. One is by integrating all nutrient components into a function to control the phytoplankton growth through simultaneous limitation of multiple nutrients [e.g., O'Neill *et al.*, 1989; Lancelot

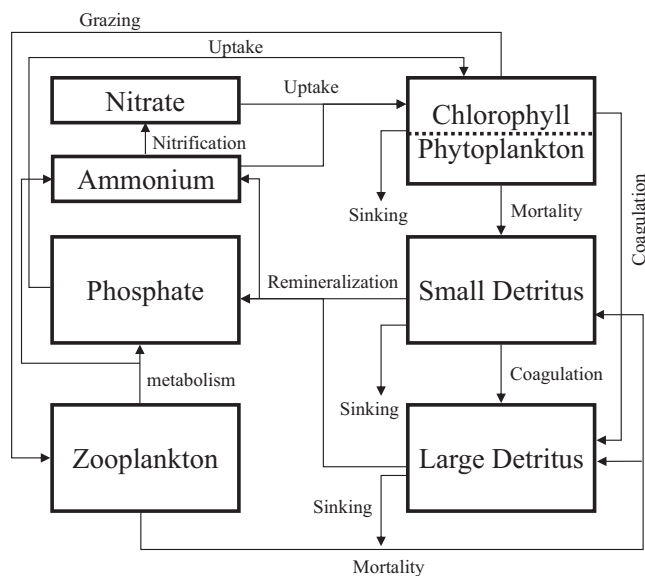


Figure 2. Schematic of the coupled physical-biogeochemical model. Boxes represent the biological variables of the model. The black solid lines with arrows indicate the biological processes between different biological variables.

et al., 2005; Lessin et al., 2007. The other widely used approach is the “minimum factor” method, where the minimum component of nutrients for controlling phytoplankton growth is adopted in the model [Guillaud *et al.*, 2000; Chen *et al.*, 2002].

In this study, we incorporated the P limitation effect into the previous N-limited model [Gan *et al.*, 2010; Lu *et al.*, 2010] by adopting the method of “minimum factor” for the nutrient function. The nutrient function for nitrogen remained unchanged and a new phosphorus function was added to reflect the P-limiting environment in the NSCS.

2. Methods

2.1. Observations

Field observations for salinity, chlorophyll-a (Chl_a), nitrate (NO₃), and phosphate (PO₄) were conducted from 30 June to 8 July 2008 aboard the R/V Shiyan III as part of SCOPE (South China Sea Coastal Oceanographic Process Experiment) [Gan *et al.*, 2010; Cao *et al.*, 2011; Han *et al.*, 2012]. The survey was a multidisciplinary research project designed to understand wind-driven coastal circulation and associated biogeochemical dynamics in the NSCS. It included the sampling of biophysical variables along seven cross-shelf transects (Figure 1). Salinity was recorded with an SBE-19-plus Conductivity-Temperature-Depth/Pressure (CTD) unit. Chl_a was determined using the fluorometric method [Parsons *et al.*, 1984]. Discrete samples for NO₃ and PO₄ were collected using a Rosette sampler with GO-FLO bottles (General Oceanics Co.), and were determined colorimetrically using a flow injection analyzer (Tri-223 autoanalyzer) [Han *et al.*, 2012].

2.2. Model and Its Implementation

The coupled physical-biological model used in this study was developed based on the Regional Ocean Modeling System (ROMS). The physical part of the ROMS is for three-dimensional, time-dependent oceanographic flows governed by hydrostatic primitive equations [Shchepetkin and McWilliams, 2005]. The local closure scheme for vertical mixing parameterization is based on the level 2.5 turbulent kinetic energy equations provided by Mellor and Yamada [1982]. The model domain extends from 15.99°N, 108.17°E in the southwest corner to about 25.81°N, 119.54°E in the northeast corner with its central axis directed 23° anticlockwise from true east (Figure 1). A curvilinear grid with a (450,140) dimensional array was adopted for horizontal coordinates (*x*, *y*) that forms a 3 km horizontal grid size, on average. The stretched, generalized, terrain following, *s*-coordinate [Song and Haidvogel, 1994] was adopted for the vertical coordinates. $\theta_s = 2.5$ and $\theta_b = 0.8$ were used in the function that defines the *s*-coordinate to give a higher vertical resolution in the surface and the bottom boundary layers. The model has 30 vertical levels that form a minimum vertical grid spacing of <1 m in the near-shore region and about 10 m over the outer shelf. The water depth, *h*(*x*, *y*), was obtained by merging ETOPO2 (1/30°) from the National Geophysical Data Center (USA) and by digitizing depths from navigation charts published by China’s Maritime Safety Administration. This is a process-oriented modeling study using simplified but specific biogeochemical/physical forcing to isolate process in the complex system. As adopted in the process-oriented coupled physical and biological simulation of Gan *et al.* [2010], upwelling was assumed to be driven entirely by a spatially uniform westerly wind stress

Table 1. Biogeochemical Model Parameters

Description	Symbol	Value	Units
Phytoplankton growth rate at 0°C	μ_0	0.59	d^{-1}
Light attenuation due to seawater	k_{water}	0.04	m^{-1}
Light attenuation by chlorophyll	k_{Chla}	0.025	$(m^2 \text{ mg Chla})^{-1}$
Initial slope of the P-I curve	α	0.025	$\text{mg C (mg Chla W m}^{-2} \text{ d)}^{-1}$
Maximum cellular chlorophyll: C ratio	θ_m	0.054	$\text{mg Chla (mg C)}^{-1}$
Cellular P:N ratio	r_{PN}	0.0625	–
Half-saturation for phytoplankton NO_3 uptake	k_N	0.8	mmol m^{-3}
Half-saturation for phytoplankton NH_4 uptake	k_A	0.8	mmol m^{-3}
Half-saturation for phytoplankton PO_4 uptake	k_P	0.06	mmol m^{-3}
Phytoplankton mortality rate	m_{phyto}	0.15	d^{-1}
Zooplankton maximum grazing rate	g_{max}	0.6	d^{-1}
Zooplankton assimilation efficiency for nitrogen	β	0.75	–
Zooplankton half-saturation constant for ingestion	k_{phyto}	1	mmol N m^{-3}
Zooplankton-basal metabolism	I_{BM}	0.1	d^{-1}
Zooplankton-specific excretion rate	L_E	0.1	d^{-1}
Zooplankton mortality rate	m_{Zoo}	0.025	$d^{-1} (\text{mmol N m}^{-3})^{-1}$
Small detritus remineralization rate for nitrogen	r_{SDN}	0.03	d^{-1}
Large detritus remineralization rate for nitrogen	r_{LDN}	0.01	d^{-1}
Small detritus remineralization rate for phosphorus	r_{SDP}	0.075	d^{-1}
Large detritus remineralization rate for phosphorus	r_{LDP}	0.025	d^{-1}
Coagulation rate	τ	0.05	d^{-1}
Sinking velocity for small detritus	w_{SD}	0.1	m d^{-1}
Sinking velocity for large detritus	w_{LD}	1	m d^{-1}
Sinking velocity for Phytoplankton	w_{phyto}	0.1	m d^{-1}
Maximum nitrification rate	n_{max}	0.05	d^{-1}
Threshold PAR for nitrification inhibition	I_0	0.0095	W m^{-2}
Half-saturation PAR for nitrification inhibition	k_I	0.036	W m^{-2}

(0.025 Pa) to represent typical NSCS summer upwelling. The model was initialized with horizontally uniform temperature and salinity profiles obtained from field measurements at station A1 (Figure 1). The model domain included two open boundaries in which open boundary conditions (OBCs) favorable to the wind-forced shelf circulation [Gan and Allen, 2005; Gan et al., 2005] were utilized on the eastern boundary. The remote forcing in the OBCs is provided by a cross-shelf two-dimensional model with reduced physics. An oblique horizontal radiation condition was applied on the southern boundary for two-dimensional and three-dimensional velocities. No-gradient condition was applied to the surface elevation in the open boundaries. The discharge rate for the Pearl River was set equal to the typical summer value of $16,500 \text{ m}^3 \text{ s}^{-1}$, and the salinity, temperature, NO_3 , and PO_4 of the river were set equal to 10 PSU, 29.5°C , 60 mmol m^{-3} , and 1 mmol m^{-3} [Cai et al., 2004], respectively, in the entire water column at the head of the PRE. More details about the physical model settings are provided in Gan et al. [2009a, 2009b].

The biological model that we developed in this study is based on a Fasham-type N-based ecosystem model [Fasham et al., 1990; Fennel et al., 2006; Hofmann et al., 2008]. To reflect the potential P limitation in the plume, three variables, phosphorus (PO_4), small phosphorus detritus (SDP), and large phosphorus detritus (LDP) are added to the original N-based model that contains seven prognostic variables: nitrate, ammonium (NH_4), chlorophyll_ *a*, phytoplankton (Phyto), zooplankton (Zoo), large detritus, and small detritus. A schematic diagram of the biological model is shown in Figure 2. The ecosystem model equations are presented in Appendix A. The parameters used in this model are listed in Table 1, the source of the parameters can be found in Fennel et al. [2006], Spitz et al. [2005], and Gan et al. [2010]. The detrital phosphorus serves a similar purpose as nitrogen detritus that can be the source of phosphorus through remineralization. At the same time, the phytoplankton growth rate in the model is determined by the nitrogen and phosphorus modules according to their respective roles in limiting biomass. In the nitrogen module, the dependence of the phytoplankton growth rate on nutrient can be written as:

$$\mu_N = f \left(\frac{[N]}{k_N + [N]} \times \frac{1}{1 + [A]/k_A} + \frac{[A]}{k_A + [A]} \right), \quad (1)$$

where μ is phytoplankton growth rate. N and A represent NO_3 and NH_4 , respectively. k_N and k_A are half-saturation constants for phytoplankton uptake by NO_3 and NH_4 , respectively. Similarly and as described in Guillard et al. [2000], the function of the growth rate in the phosphorus module is defined as:

$$\mu_p = f\left(\frac{[P]}{k_p + [P]}\right), \quad (2)$$

where P represents PO_4 and k_p is the half-saturation constant for phytoplankton uptake by PO_4 . The model switches to a lower growth rate based on the relative concentration (i.e., the ratio of μ_N/μ_P) of different nutrient species (NO_3 , NH_4 , and PO_4), or based on the N:P ratio when NH_4 is considered to be much smaller than NO_3 and PO_4 .

The N:P Redfield ratio of 16:1 is often regarded as one of the criterion for judging nutrient limitation. However, the optimum N:P ratio for phytoplankton uptake may vary from 10:1 to 30:1 for different algal species at different locations [Atkinson and Smith, 1983; Fong *et al.*, 1993]. In the eastern near-shore waters off Hong Kong, Xu *et al.* [2009] found that the optimum N:P uptake ratio of the phytoplankton community ranged from 10:1 to 16:1. The spatial and temporal trends of the N:P uptake ratio in the broad shelf region is largely unknown. In this process-oriented study, the average N:P uptake ratio ~ 13.3 is adopted, based on our recent seasonal observations conducted in the shelf region during the CHOICE-C project (a National Basic Research Program of China). Therefore, we chose the half-saturation constants for N and P to be close to the N:P ratio of 13.3:1 (Appendix A).

Despite the inclusion of PO_4 into the model, phytoplankton growth is still measured in units of nitrogen. If phytoplankton growth is limited by phosphorus, the growth is determined through the concentration of phosphorus by transforming the phosphorus into nitrogen by multiplying with a P:N ratio of 1:16. Phytoplankton growth through the consumption of N and P are both controlled by the light attenuation and the saturating concentration of nutrient. The fraction of phytoplankton consumed by zooplankton is transferred to a small detritus pool of N and P with the P:N ratio of 1:16. Coagulation of small detritus into large detritus is assimilated either as detrital P or N, respectively. Finally, large detrital N and P pools are remineralized to ammonium and phosphorus, respectively. The model separates phytoplankton and zooplankton mortality, excretion, and metabolism into N-based and P-based processes. Sinking terms are added to the small P and N detritus pools.

We obtained the initial values for the biological variables from a one-dimensional biological model and applied them uniformly in the entire model domain. The one-dimensional model was initialized with profiles of NO_3 , PO_4 , and Chl_a sampled at station A1 (Figure 1) and run for 1 year using a small background diffusivity and without phytoplankton sinking, similar to Spitz *et al.* [2005] and Gan *et al.* [2010]. Because there were no available phytoplankton, zooplankton, and detritus observations, the initial values of these parameters in the one-dimensional model were calculated from chlorophyll data by assuming a ratio of 1.59 and 0.70 for chlorophyll/phytoplankton, and detritus/phytoplankton, respectively [Evans and Garcon, 1997]. The ratio of zooplankton/phytoplankton was set to 0.3 according to observations measured in water beyond Hong Kong. We applied a radiation boundary condition to the biological variables in the open boundaries. Details about the biological model settings and conditions can be found in Gan *et al.* [2010] and Lu *et al.* [2010]. The biological model was coupled with the physical model at identical temporal and spatial resolutions. The quasi steady model outputs on day 30 are used in the analyses.

3. Results

3.1. Observational Features

During summer, the NSCS was characterized by the coexistence of the Pearl River plume (low salinity) over the middle shelf and the intensified upwelling (high salinity) on the northeast inner shelf (Figure 3a). The wind-driven alongshore currents advected freshwater eastward after it exited the PRE, while the unique widened shelf enhanced the up-slope shoreward transport and formed the intensified upwelling in the inner shelf water [Gan *et al.*, 2009a]. The physical natures of the plume from field measurements and biological responses to the physical process in the plume have been discussed in Gan *et al.* [2009b, 2010]. As a result of the high nutrient load in the plume and in the upwelled water, phytoplankton blooms occurred in these two waters (Figure 3b). The chlorophyll was very low in other regions because of the oligotrophic characteristics of the NSCS. It is noted that, although both NO_3 and PO_4 are very high in the estuary and in the deep water [Cai *et al.*, 2004], high NO_3 only existed in the plume and high PO_4 only existed in the upwelled water. PO_4 in the plume and NO_3 in the upwelled

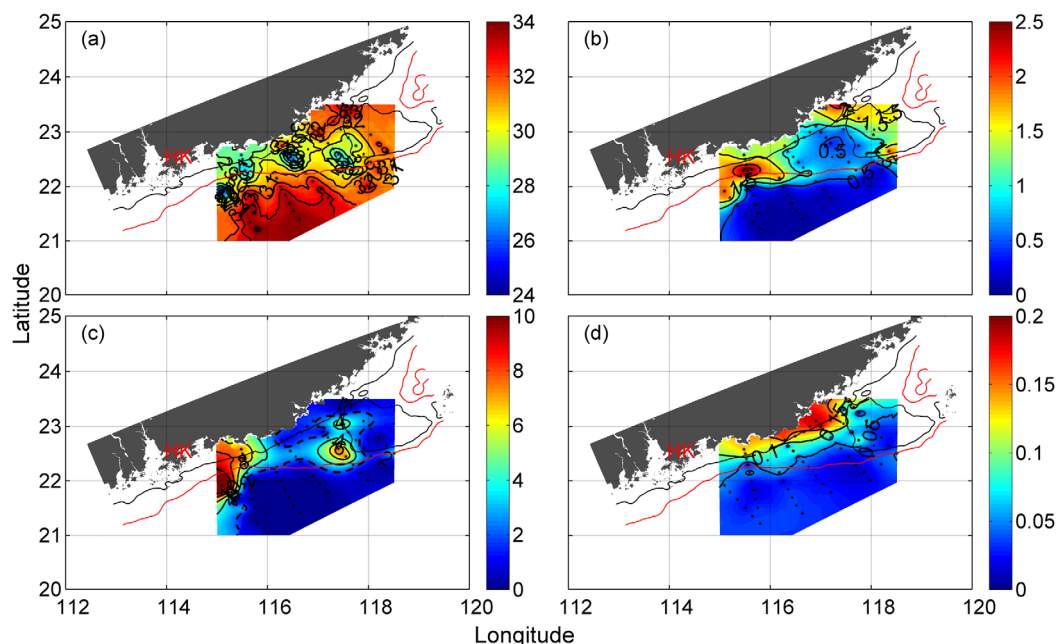


Figure 3. The surface distribution of (a) salinity, (b) chlorophyll-*a* ($\mu\text{g L}^{-1}$), (c) NO_3 ($\mu\text{mol L}^{-1}$), and (d) PO_4 ($\mu\text{mol L}^{-1}$) in the NSCS from a field measurement conducted during a summer upwelling period (30 June 2008 to 7 July 2008). The concentration of $\text{NO}_3 < 2 \mu\text{mol L}^{-1}$ is highlighted by dashed contour line. The red and black solid lines indicate the 50 and 30 m isobaths, respectively.

water were relatively low and could hardly be distinguished from the ambient oligotrophic water (Figures 3c and 3d). This suggests that PO_4 and NO_3 likely limited phytoplankton growth in the plume and in the upwelled water, respectively. An extensive description of the nutrient dynamics in the plume has been presented by Han *et al.* [2012].

3.2. Model Results

To highlight the P limitation in the Pearl River plume and to show its impact on the pelagic ecosystem of the NSCS, we compared the results from the N and P limitation (NP-based) biological model with those from N limitation alone (N-based) model. The physical and biological conditions for both cases were kept identical for consistent comparison and were the same as those reported by Gan *et al.* [2009a, 2009b, 2010]. The model results have been qualitatively validated in these previous studies.

3.2.1. Horizontal Features of the Ecosystem Response

Figure 4 shows that the southwesterly wind-driven eastward surface current bifurcates around 115.5°E , and forms a current following the 30 m isobath over the inner shelf and a relatively strong current following the 50 m isobath over the midshelf (Figure 4a). The low-salinity water from the river discharge advects eastward by the surface current and generates a prominent plume over the NSCS shelf (Figure 4b). Meanwhile, high salinity water appears over the northeastern inner shelf because of coastal upwelling. This upwelling is strong due to intensified cross-isobath bottom transport (Figure 4c), induced by dynamic forcing over the unique widened shelf (indicated by the offshore veering of the 50 m isobath). The high-salinity deep water moves up-slope crossing the isobaths near 115.5°E . It flows eastward and shoreward to form the high surface salinity water over the inner shelf (Figure 4d). Detailed hydrodynamic characteristics of the cross-isobath transport and the plume over the continental shelf of the NSCS are provided in Gan *et al.* [2009a, 2009b, 2013]. The simulated surface salinity (Figure 4b) in the plume is coherent with the upwelling current and resembles the features from the in situ measurements in Figure 3.

Two biologically active regions are formed in the river plume and in the upwelling region over the shelf, as shown by the surface Chl_a distribution in both the NP-based and N-based model results (Figure 5). These results are consistent with the in situ measurements in Figure 3 and with the results of Gan *et al.* [2010]. The development of the biologically active regions is closely coupled with the evolution of the plume and upwelling.

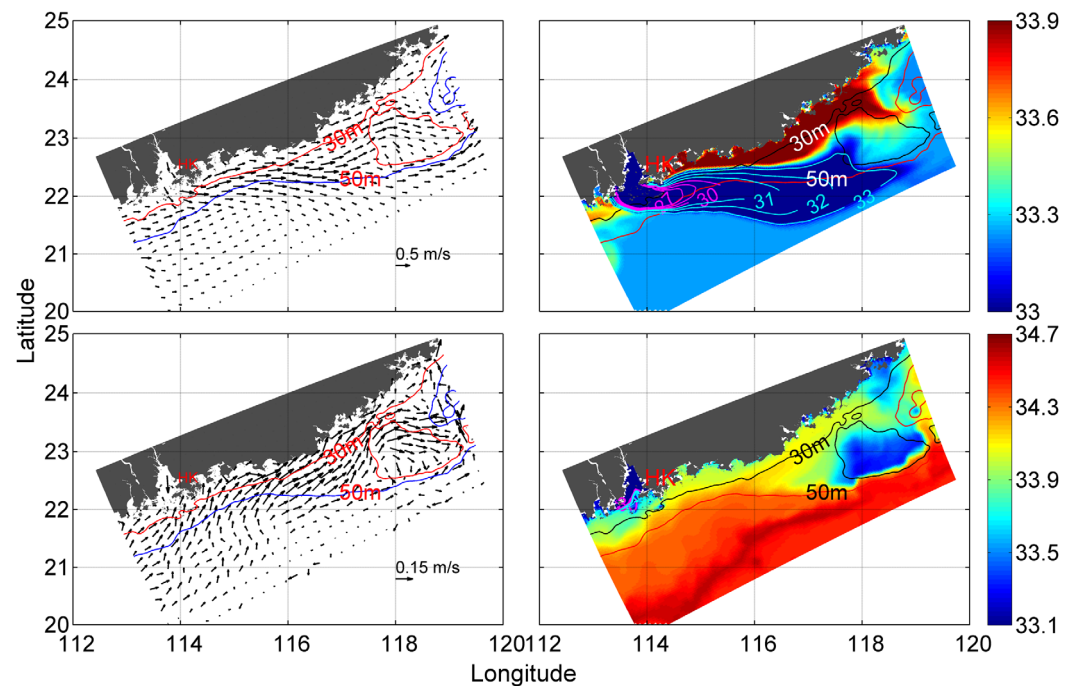


Figure 4. Surface and bottom (a,c) velocity vectors (m s^{-1}) and (b,d) salinity on day 30. See Figure 1 for geographical reference points.

During the initial stage, on day 10, the plume water leaves the freshwater bulge at the entrance of the PRE and discharges high-nutrient water onto the shelf (Figure 6). As a result, the surface Chl_a level is extremely high in the plume for both the NP-based and the N-based cases (Figures 5a and 5b). The concentrations of NO_3 and PO_4 in the estuary are both much higher than their half-saturation concentrations for phytoplankton uptake (Figure 6 and Table 1) and only weakly limit the phytoplankton growth, even though their N:P ratio is much greater than the Redfield ratio. Relatively low NO_3 and surface Chl_a occur in the upwelled water shoreward of the plume.

On day 20, although the surface Chl_a level is still fairly high in the plume in/near the estuary, Chl_a becomes relatively low in the eastward extended plume over the shelf for the NP-based case (Figures 5c and 5d). The difference between Chl_a concentration from the NP-based and N-based cases increased further on day 30 (Figures 5e and 5f). The Chl_a concentration in the NP-based case is only accounts for ~ 65 – 75% of the Chl_a in the N-based case in the near and midfield ($\sim 114^\circ\text{E}$ – 116°E) of the plume. However, the phytoplankton in the NP-based case expands farther eastward than in the N-based case and forms a relatively large phytoplankton bloom. The simulated Chl_a concentration in the NP-based case is smaller and much closer to the observed one.

Similarly, NO_3 in the NP-based case also extends farther east in the plume during all time periods (Figure 6). NO_3 consumption is expected to be reduced when the ecosystem switches from N to P limitation in the river plume due to the high N:P ratio. As a result, the surface NO_3 is always higher due to the lower biological consumption rate in the NP-based case and allows the coastal current to carry it farther east than in the N-based case (Figure 6). In contrast, there is no obvious difference of NO_3 between the NP- and N-based cases in the upwelled water. The surface distribution of PO_4 is similar to NO_3 in the near field when the plume just leaves the freshwater bulge, and PO_4 concentration keeps increasing near the entrance of the PRE due to the high-nutrient concentration in the river discharge. However, the PO_4 is decreasing quickly as the plume propagates eastward. The simulated surface distribution of NO_3 and PO_4 compares qualitatively well with the field observation (Figures 3c and 3d), in which the high NO_3 was only observed in the plume and the high PO_4 was only observed in the upwelled water.

The simulated chlorophyll/ NO_3 concentration is generally several $\mu\text{g L}^{-1}/\mu\text{mol L}^{-1}$ higher/lower than respective observed ones in the summer of year 2008 (Figure 3 versus Figures 5 and 6), particularly in the N-based case. The data in the summer 2009 (not shown), however, showed much higher/lower chlorophyll/

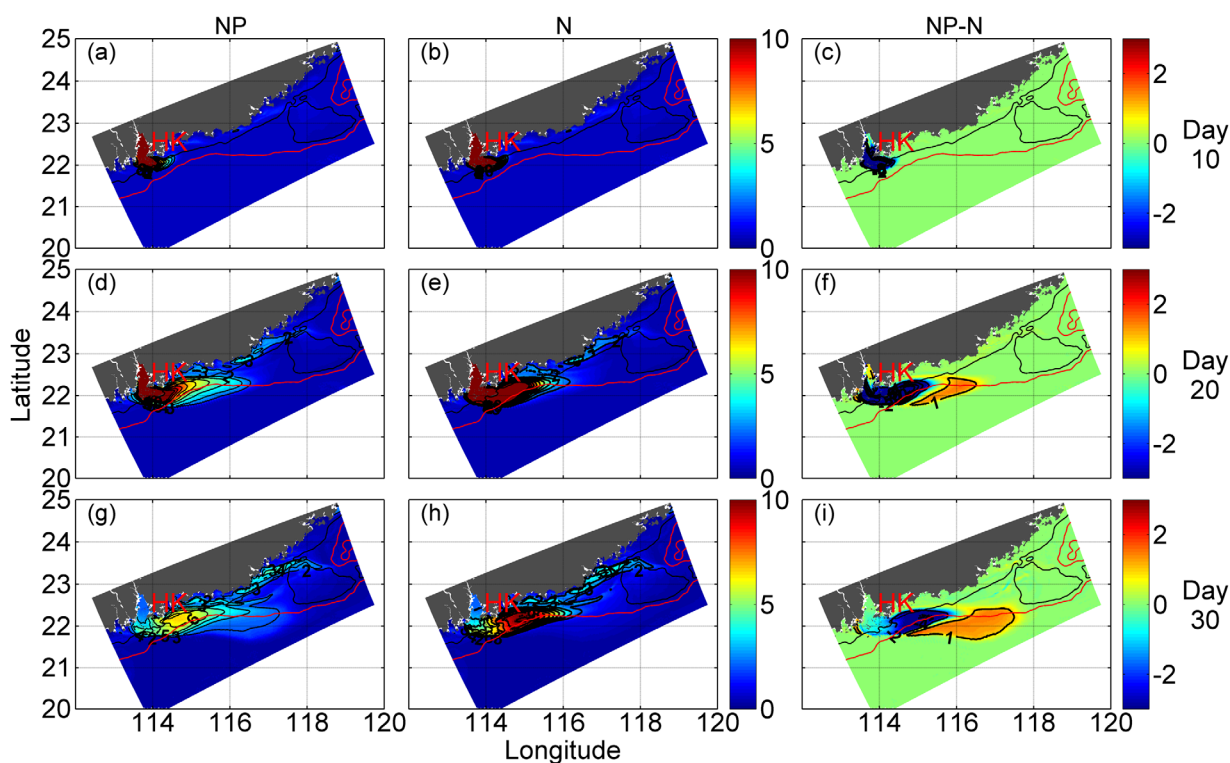


Figure 5. Surface Chl_a ($\mu\text{g L}^{-1}$) of (left column) NP-based model and (middle column) N-based model on (top) day 10, (middle) day 20, and (bottom) day 30. The right column shows the differences between NP- and N-based models.

NO_3 in the same region. The differences can be caused by many reasons, such as time-dependent and space-dependent physical and biogeochemical forcing during the survey time which is not resolved by this process-oriented study. The model also did not capture the observed patching structure of chlorophyll in the river plume, which was induced by the pulse of river discharge [Gan *et al.*, 2009a].

The growth of zooplankton depends on the phytoplankton biomass according to its growth function in the model (see equation (A5)); therefore, the horizontal distribution of zooplankton generally follows the pattern of phytoplankton to some extent (Figure 7). On day 10, there are only weak signals of zooplankton growth within/around the PRE for both cases (Figures 7a and 7b) due to the growth time lag between phytoplankton and zooplankton [Gan *et al.*, 2010; Spitz *et al.*, 2005]. The zooplankton concentration becomes higher and spreads over the shelf from day 20 to day 30 (Figures 7c–7f), along with the eastward expansion of the river plume and the phytoplankton biomass. Similar to Chl_a , the surface zooplankton biomass in the plume of the NP-based case is less than that of the N-based case because of the bottom-up control. However, the similar farther eastward extension as in Chl_a of the NP-based case does not occur for the zooplankton, which implies that the local production of zooplankton biomass in the far field is relatively small. In the upwelled water, the surface zooplankton biomass is generally $<0.2 \mu\text{mol N L}^{-1}$, analogous to the small surface Chl_a concentration due to nutrient limitation.

3.2.2. Vertical Structure of the Ecosystem

The vertical structure of the ecosystem responses in both the NP-based and N-based cases are shown in Figure 8. Sections A, B, and C from the west to the east of the shelf (Figure 1) are presented. Section A extends offshore from the PRE where the plume originates. Section B crosses the head of the widened shelf where the intensified up-slope transport and offshore veering of the plume occur. Section C is near Shantou where there is maximum upwelling in the near shore waters.

In general, there is no significant difference between the NP-based and N-based cases along section A. Similar cross-shelf structures and concentrations are found for Chl_a , NO_3 , zooplankton, and the subsurface

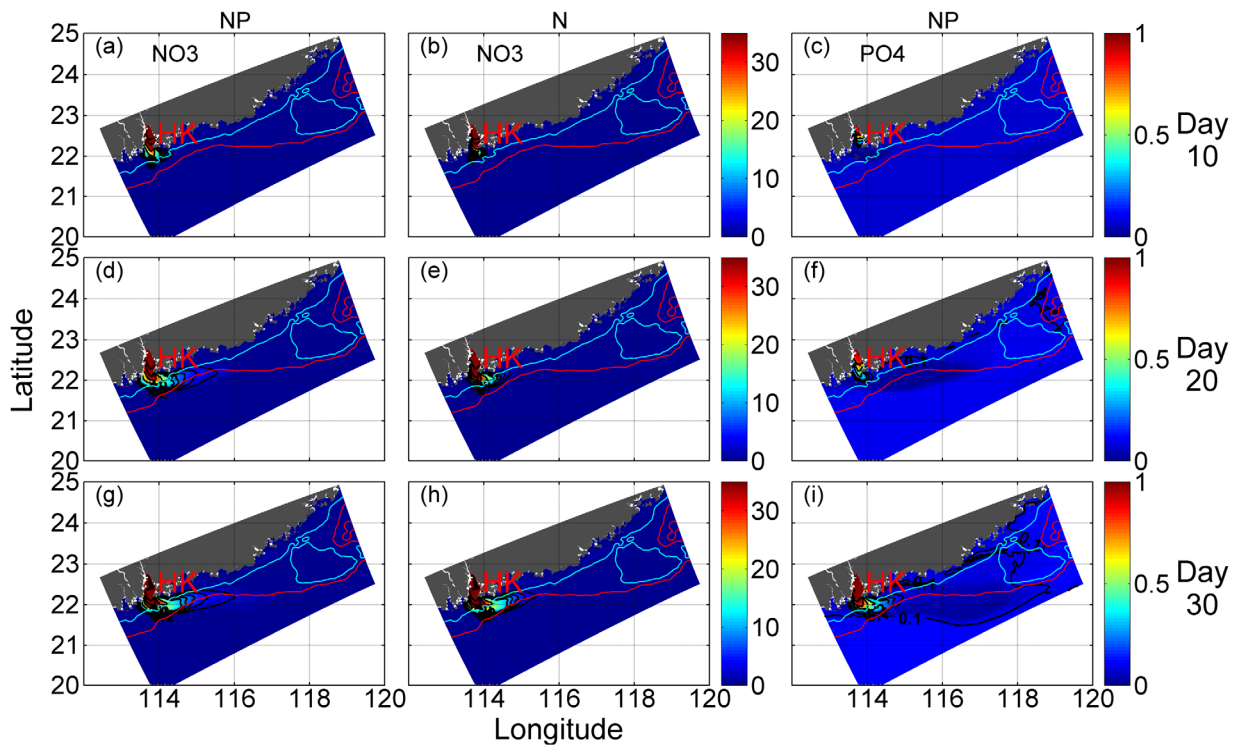


Figure 6. Surface NO_3 ($\mu\text{mol L}^{-1}$) of (left column) NP-based model and (mid column) N-based model on (top) day 10, (middle) day 20, and (bottom) day 30. The right column is surface PO_4 ($\mu\text{mol L}^{-1}$) of NP-based model on (top) day 10, (middle) day 20, and (bottom) day 30.

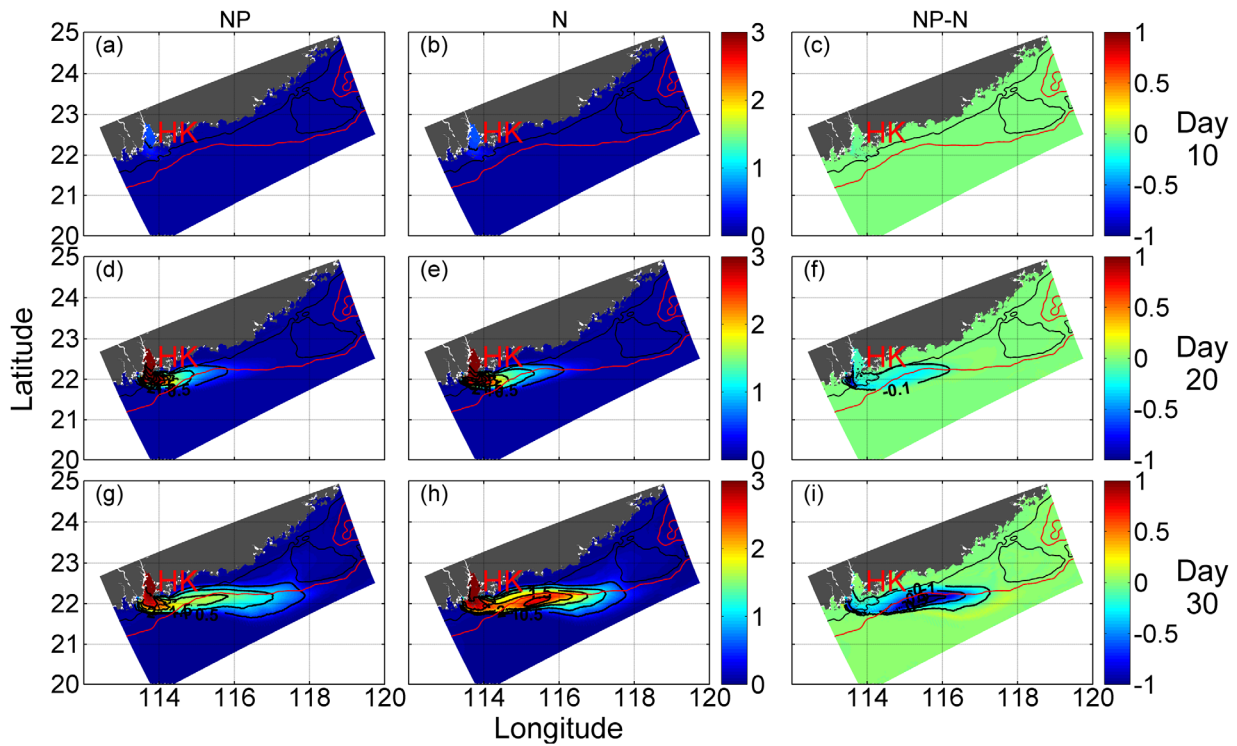


Figure 7. Surface zooplankton ($\mu\text{mol L}^{-1}$) of (left column) NP-based model and (middle column) N-based model on (top) day 10, (middle) day 20, and (bottom) day 30. The right column shows the differences between NP- and N-based models.

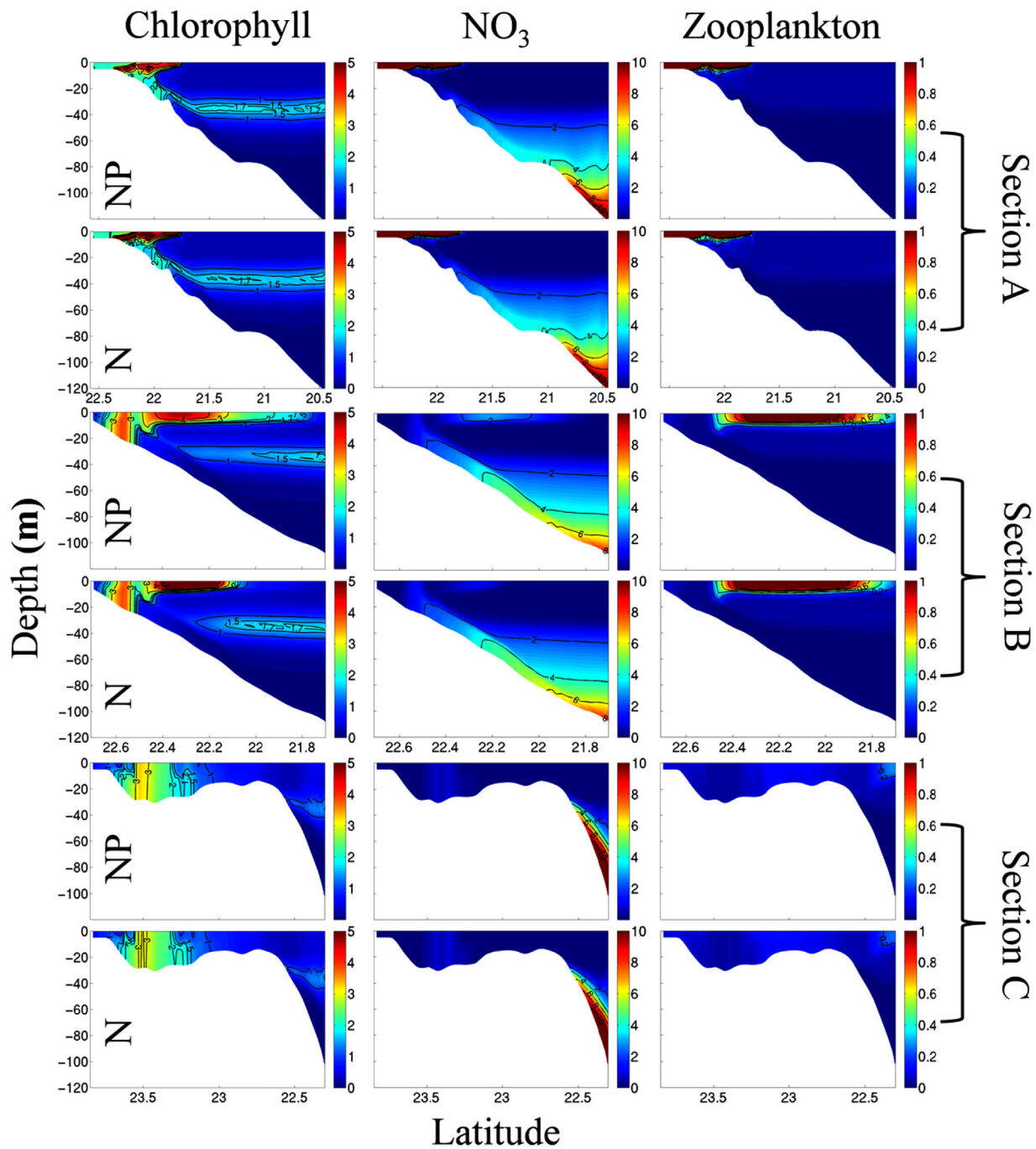


Figure 8. Cross-shore sections of (left column) chlorophyll ($\mu\text{g L}^{-1}$), (middle column) NO_3 ($\mu\text{mol L}^{-1}$), and (right column) zooplankton ($\mu\text{mol N L}^{-1}$) at sections A, B, and C (see Figure 1 for details) for the NP-based and the N-based model on day 30.

chlorophyll maximum (SCM) from 30 to 40 m (Lu et al., 2010). The most obvious difference between the cases is the lower chlorophyll level in the river plume in the NP-based case as a result of the lower phytoplankton growth rate under P limitation, which, similar to the surface chlorophyll level, is closer to the observed one.

Along section B, the river plume with high concentrations of NO_3 , phytoplankton and zooplankton extends offshore in the upper layer due to locally intensified offshore transport [Gan et al., 2009a]. The chlorophyll concentration in the plume is lower in the NP-based case than in the N-based case, while the opposite condition

occurs for NO_3 due to less biological uptake. As a result, the high surface chlorophyll water is transported farther offshore by Ekman drift in the NP-based case. Unlike in the surface layer, the SCM is stronger beneath the plume and is weaker on the offshore side for the NP-based case because Chl_a concentration is positively correlated with the corresponding photosynthetically active radiation. A similar result exists for zooplankton, but the disparity between the NP-based and N-based cases is much smaller. There is no distinct difference between the two cases for the high chlorophyll center near shore that is triggered by upwelling.

Section C is beyond the plume-influenced region and the vertical structures of all parameters are nearly identical for both N and NP cases.

While the physical field of the simulated plume and circulation are the same as those in *Gan et al.* [2009a, 2009b], the ecosystem responses and the characteristics of both horizontal and vertical fields are consistent with those obtained from the observations provided in *Han et al.* [2012] as well as in Figure 3. In particular, a non-Redfield DIN: DIP uptake ratio in the plume that leads to the differences between the NP-based and N-based model was also found by *Han et al.* [2012].

4. Analysis and Discussion

4.1. Temporal Variability of the Along-Plume N:P Ratio

When the fresh water, with a high nutrient load and a high N:P ratio, flows from the estuary, the nutrient concentration decreases quickly due to mixing with the oligotrophic ambient shelf water and biological uptake. The N:P ratio is governed by these processes over the shelf of the NSCS. The mixing process reduces the N:P ratio in the plume and equilibrium is eventually attained with the ambient water. Biological uptake enhances the N:P ratio because phytoplankton assimilates N and P at the Redfield ratio, which is lower than the N:P ratio in the river discharge. These processes can be illustrated by the time series variation of N:P ratio in the plume (salinity < 33) (Figure 9). The schematic diagrams of the N:P ratios that are regulated by idealized dilution, mixing, and biological uptake are also shown for comparison. The simulated N:P ratio in the plume increases rapidly from ~ 60 (the initial value in the river discharge) up to ~ 120 during the first 6 days, indicating that biological uptake dominates the N:P ratio in the plume at this initial stage. After that, the N:P ratio continues to decrease and gradually approaches the ambient value. This shows that mixing takes over the biological process and becomes the dominant control of the N:P ratio in the eastward spreading plume.

Effects of mixing and biological processes on the N:P ratio can also be seen in the surface distribution of the ratio (Figure 10). When the plume just exits, the PRE on day 10, phytoplankton growth is relatively high, but the intensity of mixing of the plume with ambient seawater is still limited, as also shown by the blue curve in Figure 9. Biological processes mostly control the nutrients in the plume at this time. Therefore, the N:P ratio within the plume is generally higher than its initial value (60), and almost the entire plume (the region enclosed by the contour line of salinity < 33) is P-limited (Figure 10a). Along with the eastward spreading of the plume, the N:P ratio decreases due to the strengthening of the mixing on days 20 and 30 (Figures 10b and 10c). The far field of the plume (roughly in the region between the solid yellow and dashed green lines) gradually switches from P to N deficit during this time. As mixing increases in the relatively thin plume far field [*Gan et al.*, 2009a], the area of N deficit gradually widens from day 20 to day 30 (Figures 10b and 10c). On day 30, the plume reaches $\sim 118.5^\circ\text{E}$, but the P-limited region only reaches $\sim 117.5^\circ\text{E}$, and there is a ~ 100 km spatial disparity between them. The variation in the N:P ratio along the plume is also shown in the field observations (Figure 10d), in which the N:P ratio and salinity has a negative correlation and is seldom higher than 13.3 after the salinity reaches 33.

4.2. Contrasting Evolution in the Plume

The physical forcing together with the corresponding biogeochemical processes produces the unique spatial and temporal variations in the biological variables in the plume. Figure 11 shows the time series of volume-averaged NO_3 , PO_4 , phytoplankton, and zooplankton in the plume for the NP-based and N-based cases. Both NO_3 and PO_4 concentrations and the N:P ratio are very high in the initial stage, which reflects the extremely high nutrient loading and the potential P limitation in the river water. In the NP-based case, PO_4 decreases sharply during the first 6 days when the plume water is mainly trapped in the quasi stationary freshwater bulge outside the PRE [*Gan et al.*, 2009a]. However, NO_3 remains relatively stable at the same time. In contrast, NO_3 decreases quickly in the N-based case. In the NP-based case, the high N:P ratio varies from ~ 60 to > 100 during this period and results in a relatively low consumption of NO_3 . After exiting the bulge near the entrance of the estuary on day 10, the water in the plume mixes with the ambient

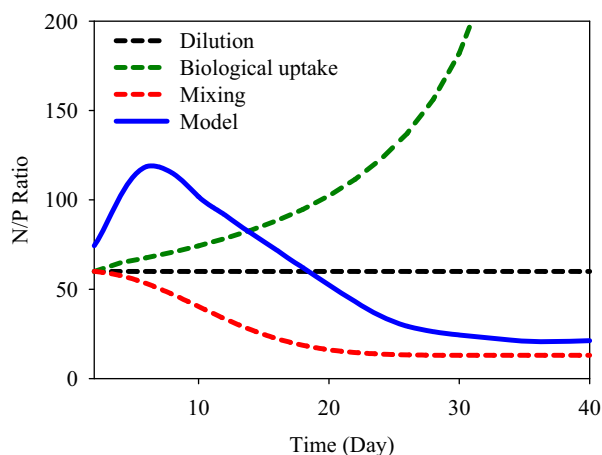


Figure 9. Time series of the volume-averaged N/P ratio in the Pearl River plume for the NP-based model (blue solid line). The volume-averaged N/P ratio is calculated by: $(N/P) = \frac{1}{V} \int_V (N/P) dV$, where V is the volume of water in plume. Also shown are schematic diagrams of the N:P ratio under pure dilution (black-dashed line, diluted with waters without nutrients); with biological uptake (green-dashed line) by assuming an uptake rate of 4.9% of total nutrients per day; and under conservative mixing with seawater in which the N:P ratio is 13 (red-dashed line) by assuming an exchange rate of 5% per day.

oligotrophic SCS water that gradually dominates the control for nutrients in the plume. Both NO_3 and PO_4 decrease, but a faster decrease occurs in NO_3 due to its relatively large difference compared to ambient water. Except during the first 10 days, the changing pattern of NO_3 in the NP-based case is very similar to that in the N-based case.

Phytoplankton also reaches its maximum on ~day 6 and attains a quasi equilibrium state around day 25 for both cases, as a result of the dynamic balance between phytoplankton growth and zooplankton grazing. However, phytoplankton biomass

is lower in the NP-based case, which demonstrates the P-limited status of the plume and its effect on the ecosystem. Generally, zooplankton biomass increases linearly before it reaches its maximum around day 24, despite the fact that phytoplankton is less than its half-saturation concentration before day 20. This is caused by the time lag between phytoplankton and zooplankton growth [Gan *et al.*, 2010; Spitz *et al.*, 2005]. The zooplankton biomass is also reduced in the NP-based case due to less phytoplankton being available for grazing because of the bottom-up control of the ecosystem by nutrients. Despite the reduction in phytoplankton and zooplankton biomass in the NP-based case, their variations are identical to those in the N-based case. As for the upwelled water, there is little difference between the NP-based and N-based cases (not shown), which suggests that the ecosystem in the upwelled water is N-limited.

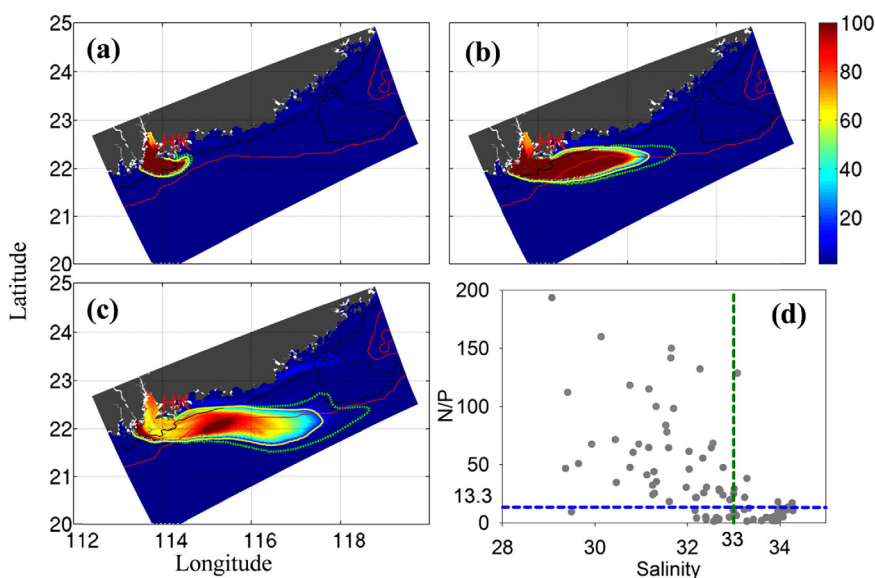


Figure 10. Surface distribution of N:P ratio for the NP-based model on days 10, 20, and 30, (a, b, and c), respectively. The yellow solid line refers to the contour of $N:P = 13.3$, the green-dotted line refers to the contour of salinity = 33. (d) is the N:P ratio versus salinity in the surface of the plume from field observations.

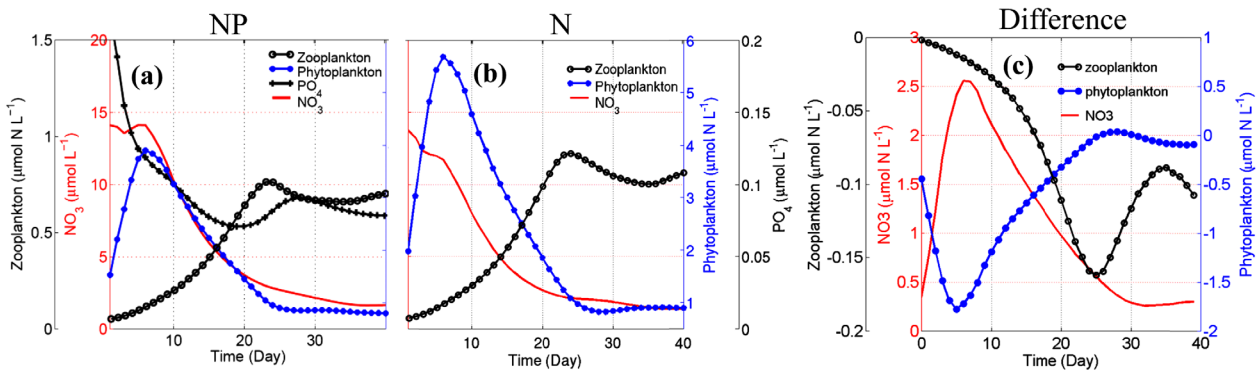


Figure 11. Time series of volume-averaged NO_3 , PO_4 , phytoplankton and zooplankton ($\mu\text{mol N L}^{-1}$) in the plume for (a) the NP-based model and (b) the N-based model. The river plume is defined as the water with salinity < 33 . The volume-averaged NO_3 , PO_4 , phytoplankton, and zooplankton are calculated by: $(N, P, \text{Phyto}, \text{Zoo}) = \frac{1}{V} \int (N, P, \text{Phyto}, \text{Zoo}) dV$, where V represents the volume of water in the plume.

4.3. Response of a River Plume Ecosystem to P Limitation

With the inclusion of P limitation, the pelagic biomass in the plume decreases compared with the N-based model, and the spatiotemporal distributions of all biochemical variables adapt to the P-limited environment. Figure 12a shows the time series of ratios of NO_3 , phytoplankton, and zooplankton in the plume between the NP- and N-based cases, which are represented by R_{NO_3} , R_{Phyto} and R_{Zoo} respectively. During the initial stage in the plume, R_{Phyto} rapidly drops from $\sim 77\%$ to its lowest value, $\sim 68\%$, on day 6 when the phytoplankton biomass reaches its maximum (Figures 11a and 11b). The disparity in the phytoplankton biomass between the two cases narrows as the plume advects eastward. With the suppression of biological consumption in the plume under P limitation in the near field, relatively high river-borne NO_3 advects farther downstream. This additional NO_3 supply to the outer part of the plume stimulates higher phytoplankton growth, as seen in the difference between Figures 12c and 12d. R_{Phyto} attains a relatively stable value of ~ 0.9 after day 35, when the plume expansion reaches a quasi steady state. With the time-averaged value of ~ 0.83 for R_{Phyto} , it suggests that the total reduction of the phytoplankton biomass is $< 20\%$ in the plume. To better illustrate the effect of P limitation, Figure 12b also shows these ratios for the upwelled water, which are ~ 1 for the entire time.

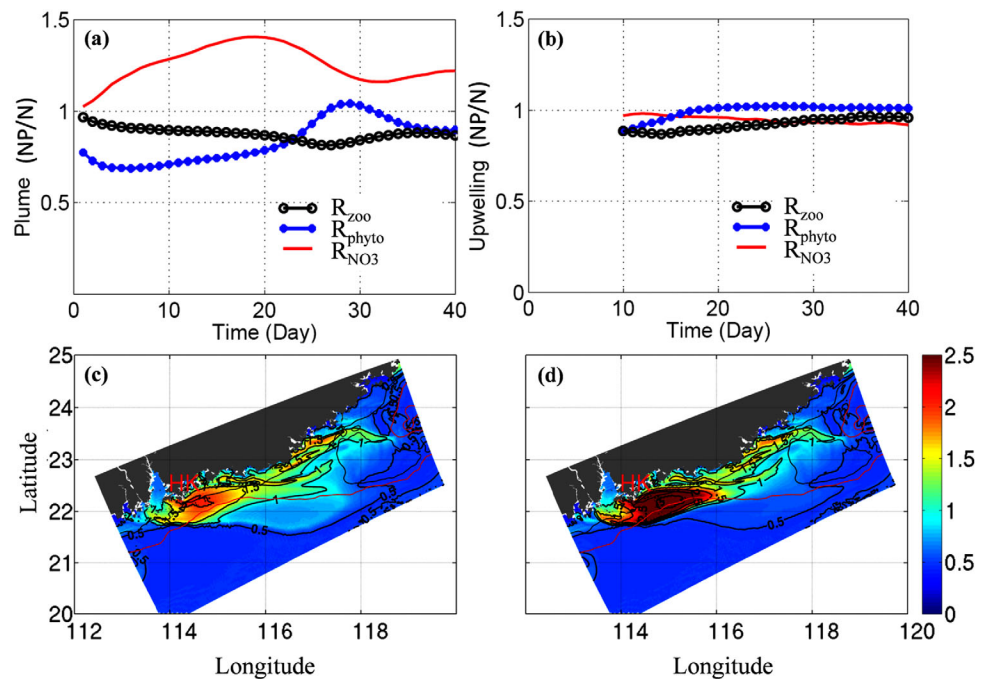


Figure 12. R_{NO_3} , R_{Phyto} and R_{Zoo} in (a) plume and (b) upwelled waters, and the surface phytoplankton ($\mu\text{mol N L}^{-1}$) on day 30 for (c) the NP-based case and (d) the N-based case.

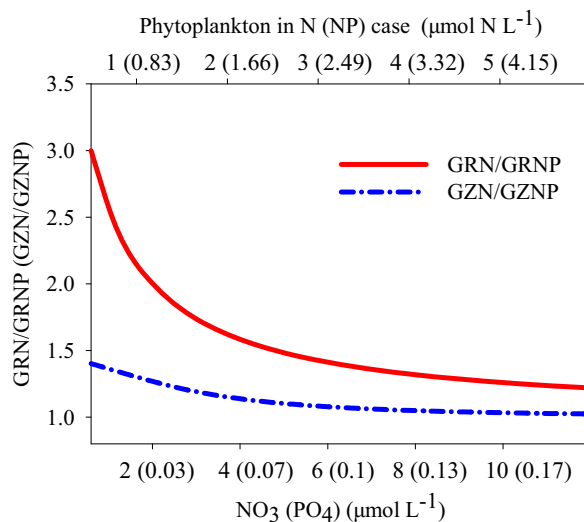


Figure 13. The ratios of phytoplankton and zooplankton growth rate between the NP-based and N-based cases as function of nutrients or phytoplankton, where GRN and GRNP represent the growth rate of phytoplankton for the N- and NP-based cases, respectively. GZN and GZNP represent the growth rate of zooplankton for the N-based and NP-based cases, respectively. The equations for calculating the growth rate of phytoplankton (A_{10}) and zooplankton (A_5) can be found in Appendix A. The variation ranges of nutrients (NO_3 and PO_4) and phytoplankton are based on model results. Since NH_4 is much less than NO_3 , for simplicity, NH_4 was neglected when we calculated the N-based phytoplankton growth rate so that the variation range of GRN/GRNP is slightly underestimated. The red solid line is the ratio of phytoplankton growth rate for the N-based and NP-based cases; the blue-dashed line is the corresponding ratio of zooplankton growth rate for the N-based and NP-based cases.

phytoplankton-nutrient and zooplankton-phytoplankton are equivalent to a kind of “buffering effect,” where the response between zooplankton and nutrients can be regarded as a “double buffering effect” that leads to the smallest variation in zooplankton biomass under different nutrient conditions during the development of the plume. Another reason is the difference in the response of the phytoplankton growth to nutrients and the response of zooplankton growth to the phytoplankton biomass. With an average N:P ratio of ~ 60 in the plume and an average R_{Phyto} of ~ 0.83 , and using the growth functions of phytoplankton (equation (A10)) and zooplankton (equation (A5)), the ratios of phytoplankton and zooplankton growth rates between the NP-based and N-based cases are shown in Figure 13. The ratio of the phytoplankton growth rate between the two cases and its variation in its range in the plume are generally larger than that of zooplankton. This is reflected in the relatively stable R_{Zoo} .

In the previous N-based model, the depth-integrated primary production (IPP) was estimated as ~ 400 – $600 \text{ mg C m}^{-2} \text{ d}^{-1}$ in the plume and contributed ~ 55 – 85% of the total IPP in the entire shelf water [Gan *et al.*, 2010]. After considering P limitation in the plume, the IPP in the NP-based model obviously decreases (Figure 14). A larger decrease ($\sim 50\%$) occurs during the early stage (\sim day 10) when the phytoplankton biomass reaches its high value (Figures 11a and 11b). As the plume waters advect eastward, the difference in the IPP between the NP-based and N-based cases decreases and their ratio increases to ~ 0.85 . The IPP increases in the periphery of the P-limited near and midfields due to the stimulation of the additional NO_3 (Figure 6). Overall, after the ecosystem reaches a mature stage, the IPP in the plume is $\sim 85\%$ of that with only N limitation. This is closer to the IPP estimated from the budget of the seawater carbonate system ($432 \pm 228 \text{ mg C m}^{-2} \text{ d}^{-1}$) [Cao *et al.*, 2011] and to the IPP estimated by the nutrient budget (M. Dai, unpublished data, 2011) based on the field data from the same cruise. There is no significant change of the IPP in the upwelled water between the NP-based and N-based cases.

4.4. Ecological Dynamics in the Plume

The spatial and temporal variation of the pelagic ecosystem is a result of interaction among different biochemical processes through a response-feedback mechanism. Figure 15 shows the time series variations of the phytoplankton growth rate, nutrient concentration, and phytoplankton biomass along the plume axis at 22.1°N for both the NP-based and N-based cases. Their respective high phytoplankton growth rate regions

Consistent variations are displayed in the time series of R_{NO_3} . It increases from ~ 1.03 on day 1 to ~ 1.41 on \sim day 19, which demonstrates the reduction of biological consumption of NO_3 under P limitation. R_{NO_3} decreases afterward when the additional NO_3 supply enhances phytoplankton growth in the plume, in the far field, outside the P-limited region. The average value of R_{NO_3} is ~ 1.25 and the difference in NO_3 between the two cases is larger than that of phytoplankton.

However, the time series variation of R_{Zoo} is much more stable, ranging from 0.81 to 0.97 with an average of 0.88. One possible reason for the stability of the variation is the response time lag among NO_3 , phytoplankton, and zooplankton [Gan *et al.*, 2010; Spitz *et al.*, 2005]. The delayed responses between

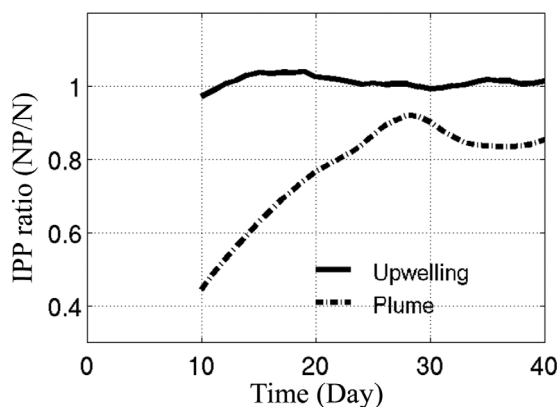


Figure 14. Time series of the depth integrated primary productivity (IPP) ratio for the NP-based and N-based models for the plume (dashed line) and in the upwelled (solid line) waters.

mainly occupy the area west of $\sim 114.8^\circ\text{E}$ and $\sim 115.3^\circ\text{E}$ (Figures 15a and 15b). Beyond this region, PO_4 is lower than its half-saturation concentration, 0.06 mmol m^{-3} , in the NP-based case (Figure 15g) and NO_3 is lower than 0.8 mmol m^{-3} in the N-based case (Figures 15e and 15d). This suggests that the pelagic ecosystem is limited by both PO_4 and NO_3 in these two regions for the NP-based and N-based cases, respectively.

Besides mixing, NO_3 is quickly exhausted along the plume in the N-based case because of the high phytoplankton growth rate that is stimulated by the very high nutrient concentration. The consumption rate of PO_4 is much slower due to the lower phytoplankton growth rate in the NP-based case. In addition, because the turnover rate (rem mineralization rate) of phosphorus is much higher than nitrogen (Table 1), the decline in PO_4 is slower than that of NO_3 in the plume (Figure 11a). This is the reason why the phytoplankton growth rate in the NP-based case is higher than that in the N-based case in the midfield region between $\sim 115.3^\circ\text{E}$ and 116.5°E . The phytoplankton growth rate in the N-based case becomes higher than that in the NP-based case east of $\sim 116.5^\circ\text{E}$ due to NH_4 replenishment from remineralization (Figure 15f).

Thus, the evolution and spatial variation of the phytoplankton biomass (Figures 15a and 15b) is explained well by the nutrient dynamics and growth function. The high phytoplankton biomass occurs about 1° farther east

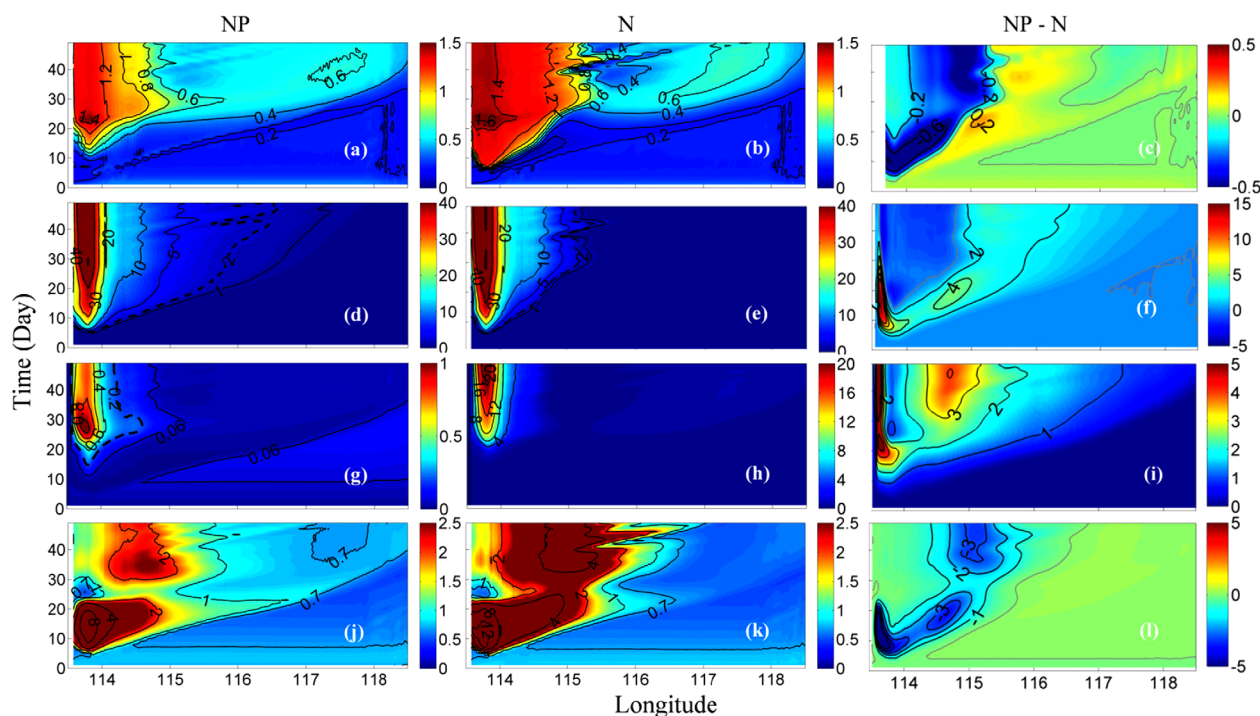


Figure 15. Time-series of surface (a, b) phytoplankton growth rate (d^{-1}), (d, e) NO_3 concentration ($\mu\text{mol L}^{-1}$), (g) PO_4 concentration ($\mu\text{mol L}^{-1}$), (h) NH_4 concentration ($\mu\text{mol L}^{-1}$), and (j, k) phytoplankton biomass ($\mu\text{mol N L}^{-1}$) along the axis of the plume (22.1°N) for (left column) NP-based and (middle column) N-based models. The right column shows the differences between NP-based and N-based models, in which, (i) shows the difference of NH_4 between NP-based and N-based models since there is no PO_4 in the N-based model. The concentration of $\text{NO}_3 = 2 \mu\text{mol L}^{-1}$ is highlighted by dashed contour line.

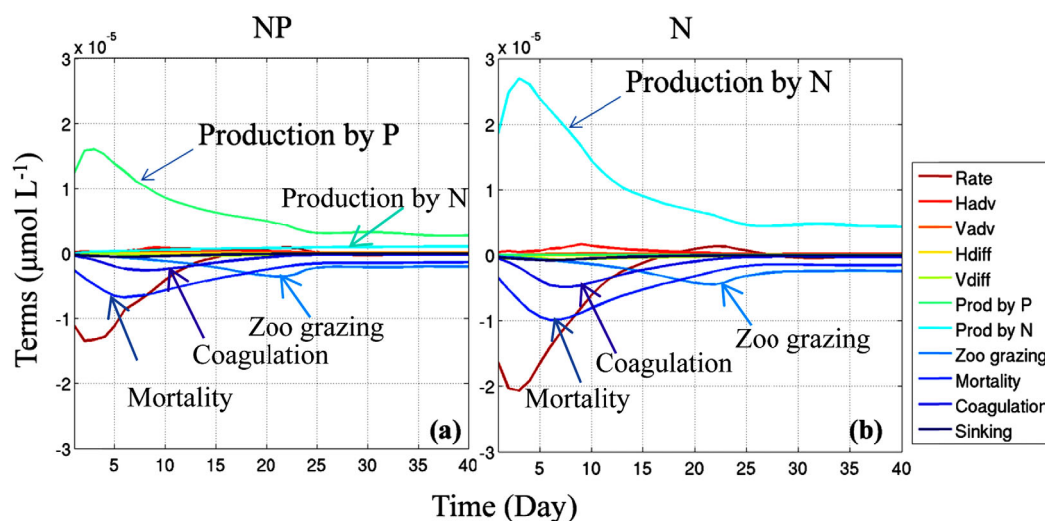


Figure 16. Time series of volume-integrated terms in the phytoplankton equation for the NP-based model and the N-based model in the plume. All terms are calculated as they are placed on the right side of the equation, such that Rate = phytoplankton variation rate increases when Rate < 0; Hadv = horizontal nonlinear advection; Vadv = vertical nonlinear advection; Hdiff = horizontal diffusion; Vdiff = vertical diffusion; Prod by P = production by phosphorus; Prod by N = production by nitrogen; Zoo grazing = zooplankton grazing.

($\sim 116.3^\circ\text{E}$) in the N-based case than in the NP-based case ($\sim 115.8^\circ\text{E}$), and the phytoplankton biomass in the N-based case is much higher than in the NP-based case in this region. However, east of $\sim 163^\circ\text{E}$, in the region between $\sim 116.3^\circ\text{E}$ and 117.5°E , the phytoplankton in the N-based case is apparently lower than in the NP-based case. The bloom occurs, generally, $\sim 1^\circ$ east of the region with high nutrients, and reflects the time lag between nutrient availability and phytoplankton biomass. With the speed of the coastal current being $\sim 0.2 \text{ m s}^{-1}$ [Gan *et al.*, 2009b] and with a spatial disparity between the phytoplankton growth rate and biomass of $\sim 103 \text{ km}$, the time lag between nutrients and phytoplankton is estimated to be ~ 6 days in the river plume.

We can also extract the evolution of the different phytoplankton responses between the NP-based and N-based cases by conducting an analysis of term balances in the phytoplankton equation (equation (A4) in Appendix A). Figure 16 shows the time series of the volume-averaged terms in the plume for these two cases. Except for the range in variation, the terms for both cases share a similar tendency. The production of PO_4 provides a large increase in phytoplankton with the maximum occurring around days 2–3 in the NP-based case. Afterward, it gradually decreases mainly under the joint regulation of mortality, coagulation, and grazing. The maximum values of mortality and coagulation have a lag of ~ 3 –5 days with respect to the production term, while phytoplankton loss by zooplankton grazing reaches its maximum on \sim day 22, about 2 days earlier than when the zooplankton reach their peak value (Figures 11a and 11b). This synthetically results from the simultaneous decrease in phytoplankton biomass and the increase in zooplankton biomass according to the grazing function.

The contributions of each term to production also vary with the evolution of the plume. During the initial stage, mortality and coagulation contributes ~ 60 –70% to the phytoplankton biomass sink; however, with increasing zooplankton, grazing becomes an important sink for phytoplankton biomass. Together with its own mortality, phytoplankton production attains a dynamic equilibrium after day 25. Similar conditions occur in the N-based case. Nevertheless, the phytoplankton production of the NP-based case (the term of production by phosphorus in the equation) only accounts for $\sim 70\%$ of the production by nitrogen in the N-based case. The small difference between zooplankton grazing in both cases suggests that nutrient limitation has less effect on zooplankton than on phytoplankton, as discussed in subsection 4.3 and illustrated in Figure 15. In the NP-based case, phytoplankton production due to nitrogen continuously increases with plume propagation. This suggests that the proportion of the N-limited area in the plume is gradually increasing, as shown by Figure 10, due to strengthened mixing at the front part of the plume.

5. Concluding Remarks

We developed a three-dimensional coupled physical-NPPZD ecosystem model based on ROMS to conduct a process-oriented study on the ecosystem response to phosphorus limitation in the Pearl River plume that

contains a high N:P ratio. We examined the contrasting biological features, ecosystem evolution, and forcing mechanism between the NP-based and N-based models, in order to extract the characteristic processes as a result of inclusion of phosphorus limitation in the plume.

We found that P limitation in the near and midfield regions of the plume regulates the ecosystem and that N limitation exists in the far field. Although the general nature of the ecosystem remains similar between the N-based case and the NP-based case, P limitation noticeably reduces the primary production in the plume, particularly in the bloom development stage.

Biological processes and physical mixing regulate the concentration of the nutrients in the developing river plume over the continental shelf. Biological uptake elevates the N:P ratio while mixing reduces it. In the near field, biological uptake is the major controlling factor and elevates the N:P ratio from its initial value of ~60 to ~120. Between the midfield and far field, physical mixing with the ambient oligotrophic seawater gradually shifts the condition from P to N deficit. As a result, the far field of the plume is N-limited. With the development of the plume over the shelf, the N-limited region in the far field increases while the size of the P-limited region remains relatively stable.

By including a P limitation module into the previous N-based ecosystem model, the biomass in the plume is reduced by ~30% at the developing stage, but the reduction is very small at the final stage (<20%). The general evolution of the ecosystem in the NP-based model is very similar to the N-based model. Because of the different growth characteristics of the phytoplankton and zooplankton, there is a buffering effect due to the delayed responses between phytoplankton-nutrients and between zooplankton-phytoplankton. Thus, we find that the degree of difference between the NP-based and N-based cases decrease sequentially in nutrients, phytoplankton, and zooplankton.

The spatiotemporal variation of the ecosystem in the plume is a result of the response-feedback mechanism among nutrients, phytoplankton, and zooplankton. In the high phytoplankton biomass region where nutrients are generally higher than their half-saturation concentration, the phytoplankton biomass of the N-based case is higher than that of the NP-based case. The opposite condition occurs in the region with relatively low phytoplankton biomass, where the NP-based case has a slower nutrient consumption rate. The major phytoplankton sink comes from mortality and coagulation during the initial stage, but along with the increase in zooplankton biomass, grazing becomes the most important sink for phytoplankton biomass. The ecosystem achieves a dynamic equilibrium at ~day 25. However, the change in zooplankton in both cases is relatively small, suggesting that zooplankton is less sensitive to nutrient conditions than phytoplankton.

This modeling study has provided the characteristic response of P limitation on the pelagic ecosystem in a plume over the continental shelf. However, a holistic understanding of ecosystem dynamics is required to further assess the effect of P limitation on the time-dependent and space-dependent ecosystem.

Appendix A

The evolution of the time-dependent biological variables in the model can be expressed by the following differential equations. There are eight prognostic variables: nitrate (N), ammonium (A), phosphate (P), chlorophyll_a (Chl), phytoplankton (Phyto), zooplankton (Zoo), large detritus (LDN, LDP), and small detritus (SDN, SDP) for NO₃ and PO₄, respectively.

$$\frac{\partial[N]}{\partial t} = -\mu_{\max} f(I)[Phyto] \left(\sigma_N \frac{[N]}{k_N + [N]} \cdot \frac{1}{1 + [A]/k_A} + \sigma_P \cdot \frac{[N]}{[N] + [A]} \cdot \frac{[P]}{k_P + [P]} \right) + n[A], \quad (A1)$$

$$\begin{aligned} \frac{\partial[A]}{\partial t} = & -\mu_{\max} f(I)[Phyto] \left(\sigma_N \frac{[A]}{k_A + [A]} + \sigma_P \cdot \frac{[A]}{[N] + [A]} \cdot \frac{[P]}{k_P + [P]} \right) - n[A] \\ & + I_{BM}[Zoo] + I_E \frac{[Phyto]^2}{k_{Phyto} + [Phyto]^2} \beta [Zoo] + r_{SDN}[SDN] + r_{LDN}[LDN], \end{aligned} \quad (A2)$$

$$\begin{aligned} \frac{\partial[P]}{\partial t} = & -\mu_{\max} f(I)[Phyto] \left(\sigma_N \left(\frac{[N]}{k_N + [N]} \cdot \frac{1}{1 + [A]/k_A} + \frac{[A]}{k_A + [A]} \right) r_{PN} + \sigma_P \frac{[P]}{k_P + [P]} r_{PN} \right) \\ & + I_{BM} r_{PN}[Zoo] + I_E r_{PN} \frac{[Phyto]^2}{k_{Phyto} + [Phyto]^2} \beta [Zoo] + r_{SDP}[SDP] + r_{LDP}[LDP], \end{aligned} \quad (A3)$$

$$\frac{\partial[\text{Phyto}]}{\partial t} = \mu[\text{Phyto}] - m_p[\text{Phyto}] - \tau([\text{SDN}] + [\text{Phyto}])[\text{Phyto}] - g_{\max} \frac{[\text{Phyto}]^2}{k_{\text{Phyto}} + [\text{Phyto}]^2} [Z] - w_{\text{Phyto}} \frac{\partial[\text{Phyto}]}{\partial z}, \quad (\text{A4})$$

$$\frac{\partial[\text{Zoo}]}{\partial t} = g_{\max} \frac{[\text{Phyto}]^2}{k_{\text{Phyto}} + [\text{Phyto}]^2} \beta[\text{Zoo}] - l_{\text{BM}}[\text{Zoo}] - l_E \frac{[\text{Phyto}]^2}{k_{\text{Phyto}} + [\text{Phyto}]^2} \beta[\text{Zoo}] - m_{\text{Zoo}}[\text{Zoo}]^2, \quad (\text{A5})$$

$$\frac{\partial[\text{SDN}]}{\partial t} = g_{\max} \frac{[\text{Phyto}]^2}{k_{\text{Phyto}} + [\text{Phyto}]^2} (1 - \beta)[\text{Zoo}] + m_{\text{Zoo}}[\text{Zoo}]^2 + m_{\text{Phyto}}[\text{Phyto}] - \tau([\text{SDN}] + [\text{Phyto}])[\text{SDN}] - r_{\text{SDN}}[\text{SDN}] - w_{\text{SD}} \frac{\partial[\text{SDN}]}{\partial z}, \quad (\text{A6})$$

$$\frac{\partial[\text{LDN}]}{\partial t} = \tau([\text{SDN}] + [\text{Phyto}])^2 - r_{\text{LDN}}[\text{LDN}] - w_{\text{LD}} \frac{\partial[\text{LDN}]}{\partial z}, \quad (\text{A7})$$

$$\frac{\partial[\text{SDP}]}{\partial t} = g_{\max} \frac{[\text{Phyto}]^2}{k_{\text{Phyto}} + [\text{Phyto}]^2} r_{\text{PN}}(1 - \beta)[\text{Zoo}] + m_{\text{Zoo}} r_{\text{PN}}[\text{Zoo}]^2 + m_{\text{Phyto}} r_{\text{PN}}[\text{Phyto}] - \tau([\text{SDN}] + [\text{Phyto}])[\text{SDP}] - r_{\text{SDP}}[\text{SDP}] - w_{\text{SD}} \frac{\partial[\text{SDP}]}{\partial z}, \quad (\text{A8})$$

$$\frac{\partial[\text{LDP}]}{\partial t} = \tau([\text{SDN}] + [\text{Phyto}]) (\text{SDP} + r_{\text{PN}} \text{Phyto}) - r_{\text{LDP}}[\text{LDP}] - w_{\text{LD}} \frac{\partial[\text{LDP}]}{\partial z}, \quad (\text{A9})$$

where μ denotes the growth rate of phytoplankton and is defined as

$$\mu = \mu_{\max} f(I) \left(\sigma_N \left(\frac{[N]}{k_N + [N]} \cdot \frac{1}{1 + [A]/k_A} + \frac{[A]}{k_A + [A]} \right) + \sigma_P \frac{[P]}{k_P + [P]} \right), \quad (\text{A10})$$

μ_{\max} is the maximum growth rate of phytoplankton under a given temperature T [Eppley, 1972]:

$$\mu_{\max}(T) = \mu_0 \cdot 1.066^T, \quad (\text{A11})$$

σ_N and σ_P are nutrient limitation coefficients, if $\frac{[N]}{k_N + [N]} \cdot \frac{1}{1 + [A]/k_A} + \frac{[A]}{k_A + [A]} > \frac{[P]}{k_P + [P]}$, denoting P limitation, then $\sigma_N = 0$ and $\sigma_P = 1$; conversely, $\sigma_N = 1$ and $\sigma_P = 0$. By considering that $[A]$ is much smaller than $[N]$ and using the values of k_N and k_P in Table 1, the N:P ratio obtained from the corresponding ratio of phytoplankton growth rate is ~ 13.3 . n is the nitrification ($\text{NH}_4^+ + 2\text{O}_2 \rightarrow \text{NO}_3^- + 2\text{H}^+ + 2\text{H}_2\text{O}$) rate that is regulated by light [Olson, 1981] and governed by the below equation in the model:

$$n = n_{\max} * \left(1 - \max \left[0, \frac{I - I_0}{k_I + I - I_0} \right] \right), \quad (\text{A12})$$

where n_{\max} is the maximum nitrification rate; I_0 is the radiation threshold for nitrification inhibition; and k_I is the half-saturation radiation for nitrification inhibition.

The function $f(I)$ represents the photosynthesis-light (P-I) relationship:

$$f(I) = \frac{\alpha I}{\sqrt{\mu_{\max}^2 + \alpha^2 I^2}}, \quad (\text{A13})$$

$$I = I(z) = I_S * PAR * \exp \left\{ -z * \left(K_{\text{water}} + K_{\text{chla}} * \int_z^0 Ch(\zeta) d\zeta \right) \right\}, \quad (\text{A14})$$

where I is the same as PAR , the photosynthetically active radiation; I_S is the incoming light just below the sea surface; α is the initial slope of the $P-I$ curve; PAR is the fraction of light that is available for photosynthesis and equals 0.43; K_{water} is the light attenuation coefficient for seawater; K_{chla} is the light attenuation coefficient for chlorophyll.

A nonlinear relationship between chlorophyll and phytoplankton biomass is applied in this model to reflect the acclimation to changes in light and nutrient conditions [Fennel *et al.*, 2006]. The model equation of chlorophyll is written as:

$$\frac{\partial[Chla]}{\partial t} = \rho_{Chla} \mu * [Chla] - m_P * [Chla] - \tau * ([SDN] + [Phyto]) * [Chla] - g_{max} * \frac{[Phyto]^2}{k_p + [Phyto]} * [Zoo] * \frac{[Chla]}{[Phyto]}^{Zoo \text{ grazing}} - W_{Phyto} \frac{\partial[Chla]}{\partial z}^{sinking}, \quad (A15)$$

where ρ_{Chla} is the fraction of phytoplankton growth that devoted to chlorophyll synthesis, which is defined as:

$$\rho_{Chla} = \frac{\theta_m * \mu * [P]}{\alpha * I * [Chla]}, \quad (A16)$$

The definitions and values of the other variables in (A1–A16) are provided in Table 1.

Acknowledgments

This research was supported by National Basic Research program (973) of China under project 2015CB954004, National Science Foundation of China under projects 41276106 and 41361164001, and by the Hong Kong Research Grant Council under project N_HKUST627/13. This work was also supported by the State Key Laboratory in Marine Pollution (SKLMP) Seed Collaborative Research Fund under project SKLMP/SCRF/0006. The field survey of the SCOPE project was co-organized by Jiang Zhu, Dongxiao Wang, Xiaogang Guo, Minhan Dai, and Jianping Gan. The data for this study are available from the corresponding author at email address: magan@ust.hk.

References

- Atkinson, M. J., and S. V. Smith (1983), C:N:P ratios of benthic marine plants, *Limnol. Oceanogr.*, *28*, 568–574.
- Cai, W. J., M. H. Dai, Y. C. Wang, W. D. Zhai, T. Huang, S. T. Chen, F. Zhang, Z. Z. Chen, and Z. H. Wang (2004), The biogeochemistry of inorganic carbon and nutrients in the Pearl River estuary and the adjacent Northern South China Sea, *Cont. Shelf Res.*, *24*(12), 1301–1319.
- Cao, Z. M., M. H. Dai, N. Zheng, D. L. Wang, Q. Li, W. D. Zhai, F. F. Meng, and J. P. Gan (2011), Dynamics of the carbonate system in a large continental shelf system under the influence of both a river plume and coastal upwelling, *J. Geophys. Res.*, *116*, G02010, doi:10.1029/2010JG001596.
- Chen, C. S. *et al.* (2002), A model study of the coupled biological and physical dynamics in Lake Michigan, *Ecol. Modell.*, *152*(2-3), 145–168, Pii:S0304-3800(02)00026-1.
- Eppley, R. W. (1972), Temperature and phytoplankton growth in sea, *Fish Bull.*, *70*(4), 1063–1085.
- Evans, G. T., and V. C. Garçon (1997), One-dimensional models of water column biogeochemistry, *JGOFs Rep.* 23/97, 85 pp., JGOFs, Bergen, Norway.
- Fasham, M. J. R., H. W. Ducklow, and S. M. McKelvie (1990), A nitrogen-based model of plankton dynamics in the oceanic mixed layer, *J. Mar. Res.*, *48*, 591–639.
- Fennel, K., J. Wilkin, J. Levin, J. Moisan, J. O'Reilly, and D. Haidvogel (2006), Nitrogen cycling in the Middle Atlantic Bight: Results from a three-dimensional model and implications for the North Atlantic nitrogen budget, *Global Biogeochem. Cycles*, *20*, GB3007, doi:10.1029/2005GB002456.
- Fong, P., J. B. Zedler, and R. M. Donohoe (1993), Nitrogen vs phosphorus limitation of algal biomass in shallow coastal lagoons, *Limnol. Oceanogr.*, *38*(5), 906–923.
- Gan, J., and J. S. Allen (2005), On open boundary conditions for a limited-area coastal model off Oregon. Part 1: Response to idealized wind forcing, *Ocean Modelling*, *8*(1-2), pp. 115–133, doi:10.1016/j.ocemod.2003.12.006.
- Gan, J., J. S. Allen, and R. Samelson (2005), On open boundary conditions for a limited-area coastal model off Oregon. Part 2: Response to wind forcing from a regional mesoscale atmospheric model, *Ocean Modelling*, *8*(1-2), pp. 155–173, doi:10.1016/j.ocemod.2003.12.007.
- Gan, J., L. Li, D. X. Wang, and X. G. Guo (2009a), Interaction of a river plume with coastal upwelling in the northeastern South China Sea, *Cont. Shelf Res.*, *29*(4), 728–740, doi:10.1016/j.csr.2008.12.002.
- Gan, J., A. Cheung, X. G. Guo, and L. Li (2009b), Intensified upwelling over a widened shelf in the northeastern South China Sea, *J. Geophys. Res.*, *114*, C09019, doi:10.1029/2007jc004660.
- Gan, J., Z. M. Lu, M. H. Dai, A. Cheung, P. Harrison, and H. B. Liu (2010), Biological response to intensified upwelling and to a river plume in the northeastern South China Sea: A modeling study, *J. Geophys. Res.*, *115*, C09001, doi:10.1029/2009JC005569.
- Gan, J., J. J. Wang, L. L. Liang, L. Li, and X. G. Guo (2014), A modeling study of the formation, maintenance, and relaxation of upwelling circulation on the northeastern South China Sea Shelf, *Deep Sea Res., Part II*, doi:10.1016/j.dsr2.2013.12.009.
- Guillaud, J. F., F. Andrieux, and A. Menesguen (2000), Biogeochemical modelling in the Bay of Seine (France): An improvement by introducing phosphorus in nutrient cycles, *J. Mar. Syst.*, *25*(3-4), 369–386.
- Han, A., M. Dai, S. Kao, J. Gan, Q. Li, L. Wang, W. Zhai and L. Wang (2012), Nutrient dynamics and biological consumption in a large continental shelf system under the influence of both a river plume and coastal upwelling, *Limnol. Oceanogr.*, *57*(2), 486–502, doi:10.4319/lo.2012.57.2.0486.
- Harrison, P. J., M. H. Hu, Y. P. Yang, and X. Lu. (1990). Phosphate limitation in estuarine and coastal waters of China. *J. Exp. Mar. Biol. Ecol.*, *140*, 79–87.
- Harrison, P. J., K. D. Yin, J. H. W. Lee, J. P. Gan, and H. B. Liu (2008), Physical-biological coupling in the Pearl River Estuary, *Cont. Shelf Res.*, *28*(12), 1405–1415, doi:10.1016/j.csr.2007.02.011.
- Hofmann, E. *et al.* (2008), Eastern U.S. Continental Shelf Carbon Budget Integrating Models, Data Assimilation, and Analysis, *Oceanography*, *21*(1), 86–104.
- Howarth, R. W. (1988), Nutrient limitation of net primary production in marine ecosystems, *Annu. Rev. Ecol. Syst.*, *19*, 89–110.
- Lancelot, C., Y. Spitz, N. Gypens, K. Ruddick, S. Becquevort, V. Rousseau, G. Lacroix, and G. Billen (2005), Modelling diatom and Phaeocystis blooms and nutrient cycles in the Southern Bight of the North Sea: The MIRO model, *Mar. Ecol. Prog. Ser.*, *289*, 63–78.
- Lessin, G., I. Lips, and U. Raudsepp (2007), Modelling nitrogen and phosphorus limitation on phytoplankton growth in Narva Bay, south-eastern Gulf of Finland, *Oceanologia*, *49*(2), 259–276.
- Lu, Z. M., and J. P. Gan (2014), Controls of seasonal variability of phytoplankton blooms in the Pearl River Estuary, *Deep Sea Res. II*, doi:10.1016/j.dsr2.2013.12.011.
- Lu, Z. M., J. P. Gan, M. H. Dai, and A. Y. Y. Cheung (2010), The influence of coastal upwelling and a river plume on the subsurface chlorophyll maximum over the shelf of the northeastern South China Sea, *J. Mar. Syst.*, *82*(1-2), 35–46, doi:10.1016/j.jmarsys.2010.03.002.

- Mellor, G. L., and T. Yamada (1982), Development of a turbulence closure-model for geophysical fluid problems, *Rev. Geophys.*, *20*(4), 851–875.
- Ning, X., F. Chai, H. Xue, Y. Cai, C. Liu, and J. Shi (2004), Physical-biological oceanographic coupling influencing phytoplankton and primary production in the South China Sea, *J. Geophys. Res.*, *109*, C10005, doi:10.1029/2004JC002365.
- O'Neill, R. V., D. L. Deangelis, J. J. Pastor, B. J. Jackson, and W. M. Post (1989), Multiple nutrient limitations in ecological models, *Ecol. Modell.*, *46*(3–4), 147–163.
- Olson, R. J. (1981), Differential photoinhibition of marine nitrifying bacteria: A possible mechanism for the formation of the primary nitrite maximum, *J. Mar. Res.*, *39*(2), 227–238.
- Parsons, T. R., Y. Maita, and C. M. Lalli (1984), *A Manual of Chemical and Biological Methods for Seawater Analysis*, Pergamon, Oxford, U. K.
- Redfield, A. C. (1958), The biological control of chemical factors in the environment, *Am. Sci.*, *46*, 205–211.
- Shchepetkin, A. F., and J. C. McWilliams (2005), The regional oceanic modeling system (ROMS): A split-explicit, free-surface, topography-following-coordinate oceanic model, *Ocean Modell.*, *9*(4), 347–404, doi:10.1016/j.ocemod.2004.08.002.
- Song, Y. H., and D. Haidvogel (1994), A semiimplicit ocean circulation model using a generalized topography-following coordinate system, *J. Comput. Phys.*, *115*(1), 228–244.
- Spitz, Y. H., J. S. Allen, and J. Gan (2005), Modeling of ecosystem processes on the Oregon shelf during the 2001 summer upwelling, *J. Geophys. Res.*, *110*, C10S17, doi:10.1029/2005JC002870.
- Wu, J. F., S. W. Chung, L. S. Wen, K. K. Liu, Y. L. L. Chen, H. Y. Chen, and D. M. Karl (2003), Dissolved inorganic phosphorus, dissolved iron, and Trichodesmium in the oligotrophic South China Sea, *Global Biogeochem. Cycles*, *17*(1), 1008, doi:10.1029/2002GB001924.
- Xu, J., K. Yin, L. He, X. C. Yuan, A. Y. T. Ho, and P. J. Harrison (2008), Phosphorus limitation in the northern South China Sea during the late summer: Influence of the Pearl River, *Deep Sea Res., Part I*, *55*, 1330–1342.
- Xu, J., K. D. Yin, A. Y. T. Ho, J. H. W. Lee, D. M. Anderson, and P. J. Harrison (2009), Nutrient limitation in Hong Kong waters inferred from comparison of nutrient ratios, bioassays and P-33 turnover times, *Mar. Ecol. Prog. Ser.*, *388*, 81–97.
- Xue, H., and F. Chai (2002), Coupled physical-biological model for the Pearl River Estuary: A phosphate limited subtropical ecosystem, in *Estuarine and Coastal Modeling: Proceedings of the Seventh International Conference, 5–7 November 2001, St. Petersburg, Florida*, edited by M. L. Spaulding, pp. 913–928, Am. Soc. of Civ. Eng., Reston, Va.
- Yin, K. D. (2002), Monsoonal influence on seasonal variations in nutrients and phytoplankton biomass in coastal waters of Hong Kong in the vicinity of the Pearl River estuary, *Mar. Ecol. Prog. Ser.*, *245*, 111–122.
- Zhang, J. (2000), Evidence of trace metal limited photosynthesis in eutrophic estuarine and coastal waters, *Limnol. Oceanogr.*, *45*(8), 1871–1878.